Instructions for use

In Situ Electrochemical, Electrochemical Quartz Crystal Microbalance, Scanning Tunneling Microscopy, and Surface X-ray Scattering Studies on Ag/AgCl Reaction at the Underpotentially Deposited Ag Bilayer on the Au(111) Electrode Surface

Kohei Uosaki,[*,†,‡] Jun Morita,[‡] Tomoko Katsuzaki,[‡] Satoru Takakusagi,[‡] Kazuhisa Tamura,[§] Masamitu Takahasi,[§] Jun'ichiro Mizuki,[§] and Toshihiro Kondo[*,∥]

[†]International Center for Materials Nanoarchitectonics (MANA), National Institute for Materials Science (NIMS), Namiki, Tsukuba, Ibaraki 305-0044, Japan

[‡]Division of Chemistry, Graduate School of Science, Hokkaido University, Sapporo 060-0810, Japan

[§]Japan Atomic Energy Agency, Koto, Sayo-cho, Hyogo 679-5148, Japan

[∥]Division of Science, Graduate School of Humanities and Sciences, Ochanomizu University, Ohtsuka, Bunkyo-ku, Tokyo 112-8610, Japan

ABSTRACT: Ag/AgCl reaction at the Ag bilayer, which was underpotentially prepared on a Au(111) surface, was investigated using electrochemical quartz crystal microbalance (EQCM), scanning tunneling microscopy (STM), surface X-ray scattering (SXS), and electrochemical techniques. When the potential was scanned positively from -200 mV, the Cl^- ion was adsorbed on the Au(111) electrode surface around 0 mV, and then the phase transition of the adsorbed Cl^- ion layer from random orientation to $(\sqrt{3} \times \sqrt{3})$ structure took place at around $+130$ mV. The Ag bilayer and Cl^- ions were oxidatively reacted to form the AgCl monolayer with $(\sqrt{13} \times \sqrt{13})R13.9°$ structure around $+200$ mV, accompanied with the formation of AgCl monocrystalline clusters on the AgCl monolayer surface. The structure of the AgCl monolayer on the Au(111) surface was changed from $(\sqrt{13} \times \sqrt{13})R13.9°$ structure to (4×4) structure around $+500$ mV. When the potential was scanned back negatively, the AgCl monolayer was electrochemically reduced, and a Ag monolayer, not a bilayer, was formed on the Au(111) surface. In the subsequent potential cycles, the structural change between the Ag monolayer and the AgCl monolayer was reversibly observed. All oxidative structural changes were much slower than the reductive ones.
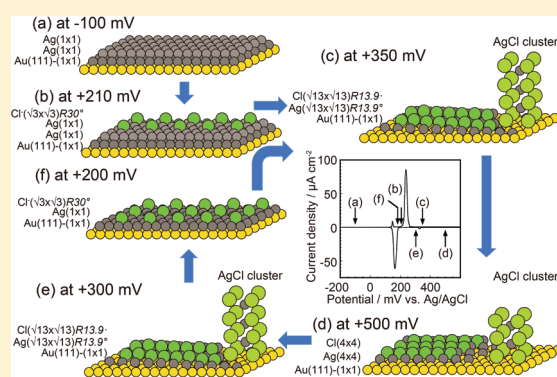
I. INTRODUCTION

To fully understand the mechanisms of electrochemical reactions and to apply these reactions to modern nanotechnology such as fuel cells, sensors, and molecular devices, it is very important to know the structures at the electrode/electrolyte interfaces in situ in real time with an atomic resolution. Scanning probe microscopy (SPM) including scanning tunneling microscopy (STM) and atomic force microscopy (AFM), surface X-ray scattering (SXS), electrochemical quartz crystal microbalance (EQCM), and several surface-sensitive spectroscopic techniques are often used to investigate the structures at the electrochemical interfaces at atomic levels.[1,2]

It is well-known that physical and chemical properties of an ultrathin metal layer on a foreign substrate are different from those of the bulk metal.[3,4] The establishment of preparation methods of ultrathin metal films with ordered structures and understanding of the origin of their unique physical and chemical properties are very important for both fundamental science and industrial applications. The epitaxial growth of well-defined thin metal layers has been achieved by vapor deposition, molecular

beam epitaxy (MBE), and metalorganic chemical vapor deposition (MOCVD) under vacuum condition.[5−7] Compared with the deposition of metals by these vacuum techniques, electrochemical metal deposition and electrochemical modulation of surface atomic structure are economical and easy because expensive and complicated vacuum equipment is not required for these electrochemical techniques. Previously, we have demonstrated that electrochemically deposited Pd ultrathin films on Au(111) and Au(100) surfaces are epitaxial with pseudomorphic structure to the substrate structure by using in situ STM and SXS techniques and discussed the relationship between the interfacial structures and the electrochemical properties.[8−14] We have also studied the structure of an underpotentially deposited (UPD) Ag ultrathin layer on a Au(111) surface using in situ SXS technique and proved that the UPD Ag layer on Au(111) is pseudomorphic mono- and bilayers at 50 and 10 mV
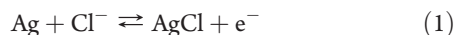
(vs Ag/Ag$^+$), respectively,[15] and the structure of the Ag bilayer is intact even after the circuit was disconnected and the surface exposed to ambient atmosphere.[16]

Ag/AgCl reaction (eq 1) is one of the most fundamental reactions in electrochemistry and is a basis for a Ag/AgCl reference electrode.

$$Ag + Cl^- \rightleftharpoons AgCl + e^- \qquad (1)$$

Moreover, the silver halides have been playing an important role in photography. There are, however, no reports about Ag/AgCl reaction at an atomic level, although several structural studies on a Cl monolayer on a Ag single crystal surface with atomic resolution are available.[17−35] This is because when potential is made positive so that the chlorination reaction (forward reaction of eq 1) proceeds at the Ag single crystal electrode the reaction takes place not only at the surface but also at the bulk, and the aggregates of AgCl clusters, in which atomic arrangements should be random, are formed. Furthermore, the electrochemical reduction of AgCl does not result in an atomically flat single crystalline Ag surface.

Here, we were able to investigate the Ag/AgCl reaction at an atomic level for the first time by using the Ag bilayer prepared by UPD on Au(111) (Ag(2ML)/Au(111)) as a substrate. Electrochemical quartz crystal microbalance (EQCM), scanning tunneling microscopy (STM), surface X-ray scattering (SXS), and electrochemical techniques were used. When potential was scanned positively, the Cl$^-$ ion was adsorbed on the electrode surface around 0 mV, and then the phase transition of the adsorbed Cl$^-$ ion layer from random orientation to ($\sqrt{3} \times \sqrt{3}$) structure took place at +130 mV. When the potential was made more positive, the Ag bilayer was oxidatively reacted with the Cl$^-$ ion to form the AgCl monolayer around +200 mV, accompanied with a formation of AgCl monocrystalline clusters. STM and SXS investigations showed that the structure of the AgCl monolayer on Au(111) was ($\sqrt{13} \times \sqrt{13}$)$R13.9°$ at +350 mV and was converted to (4 × 4) at +500 mV. When the potential was made negative, the (4 × 4) structure was converted to ($\sqrt{13} \times \sqrt{13}$)$R13.9°$ around +330 mV, and then the AgCl monolayer was electrochemically reduced around +180 mV to the Ag monolayer, not bilayer, with a small amount of AgCl clusters on the Au(111) surface. In the following potential cycles, a reversible structure change between the Ag monolayer and the AgCl monolayer was observed. All the oxidative structural changes were much slower than the reductive ones.

II. EXPERIMENTAL SECTION

Materials. Au(111) single crystal disks (diameter, 10 mm; thickness, 5 mm) were purchased from Surface Preparation Laboratory. Gold, platinum, silver, and titanium wires were purchased from Nilaco. A 5 MHz AT-cut quartz crystal plate (diameter, 13 mm; double side polished) was obtained from Fine Crystals. Ultrapure reagent grade H$_2$SO$_4$ and HClO$_4$ and reagent grade NaCl and Ag$_2$SO$_4$ were purchased from Wako Pure Chemicals and were used without further purification. Water was purified using a Milli-Q system (Yamato, WQ-500). Ultrapure N$_2$ (99.9995%), Ar (99.999%), and H$_2$ (99.99%) were purchased from Air Water.

Electrochemical Measurements. A Au(111) disk was used as a working electrode after being electrochemically etched in a 0.1 M HClO$_4$ aqueous solution containing 5 mM NaCl[36] then annealed at 850 °C for 10 h under Ar atmosphere in an electrical furnace (Denken, KDF S-70). A Pt wire (diameter: 0.3 mm) and a Ag/Ag$^+$ or Ag/AgCl (sat. NaCl) electrode were used as a counter and a reference electrode, respectively. The electrode potential was controlled by a potentiostat/galvanostat (Hokuto Denko, HA-151), and an external potential was provided by a function generator (Hokuto Denko, HB-111). Cyclic voltammograms (CVs) were recorded on an X−Y recorder (Graphtech, WX1200).

Prior to Ag UPD, the Au(111) disk electrode was annealed using a Bunsen burner or a hydrogen flame, cooled in a quartz vessel for a few minutes, and then quenched in ultrapure water.[37,38] It was then transferred to a conventional electrochemical cell with a drop of ultrapure water on the surface to avoid any surface contamination. Only the (111) face was contacted to a deaerated 50 mM H$_2$SO$_4$ aqueous solution containing 1 mM Ag$_2$SO$_4$ while keeping the potential at +700 mV (vs Ag/Ag$^+$), where no Ag is electrodeposited. The Ag UPD bilayer (Ag(2 ML)) on the Au(111) electrode surface was electrochemically prepared by scanning the potential from +700 to +10 mV with a scan rate of 5 mV s^{-1}.[15] After preparation of the Ag UPD bilayer on the Au(111) surface, the Ag(2 ML)/Au(111) disk was rinsed in ultrapure water, dried by blowing ultrapure N$_2$ gas, and then transferred to another electrochemical cell filled with 50 mM H$_2$SO$_4$ aqueous solution containing a given amount of NaCl while keeping the potential at −200 mV (vs Ag/AgCl), which was more negative than the potential where any anodic peaks were observed.[16] Only the Ag(2 ML)/Au(111) electrode surface made contact with the electrolyte solution, i.e., in meniscus configuration, and then the Ag/AgCl reaction was carried out by scanning the potential negatively.

EQCM Measurements. Au electrodes for the EQCM measurements were prepared by vacuum evaporation of 3 nm Ti followed by 150 nm Au on both sides of the quartz crystal plate at 300 °C at an evaporation rate of ca. 0.5 nm s^{-1}.[39] One of the Au electrodes was used as a working electrode. The quartz plate with electrodes was mounted in a homemade EQCM resonator. A Pt wire (diameter: 0.5 mm) and Ag/AgCl (sat. NaCl) electrode were used as a counter and a reference electrode, respectively. The resonant frequency of the quartz crystal electrode, which was oscillated by a homemade oscillation circuit, was monitored by a frequency counter (Hewlett-Packard, HP53132A). The frequency stability of the EQCM system was better than 0.1 Hz for a sampling gate time of 0.1 s.[39] The mass change (Δm) was estimated from the resonant frequency change (Δf) by the Sauerbrey equation[40]

$$\Delta m = -k \times \Delta f \qquad (2)$$

where k is the mass sensitivity of the AT-cut quartz crystal and was determined to be 19.3 ng cm^{-2} Hz^{-1} by measuring the $\Delta m - \Delta f$ relations for the deposition reactions of Ag and Pb.[39]

Prior to Ag UPD, the Au film on the quartz plate was annealed by a Bunsen burner and quenched in ultrapure water. Ag (2 ML) was deposited on the Au film electrode in an EQCM cell filled with a deaerated 50 mM H$_2$SO$_4$ aqueous solution containing 1 mM Ag$_2$SO$_4$ by scanning the potential from +1000 mV (vs Ag/AgCl) to +480 mV with a scan rate of 5 mV s^{-1}.[15] After rinsing and drying the Ag(2 ML)/Au film electrode with ultrapure water and by blowing ultrapure N$_2$ gas, respectively, the Ag(2 ML)/Au film electrode was set to the EQCM cell, and the Ag/AgCl reaction was carried out in a 50 mM H$_2$SO$_4$ aqueous solution containing 2 mM NaCl by scanning the potential between −220 and +500 mV.

12472

dx.doi.org/10.1021/jp2010502 |J. Phys. Chem. C 2011, 115, 12471–12482
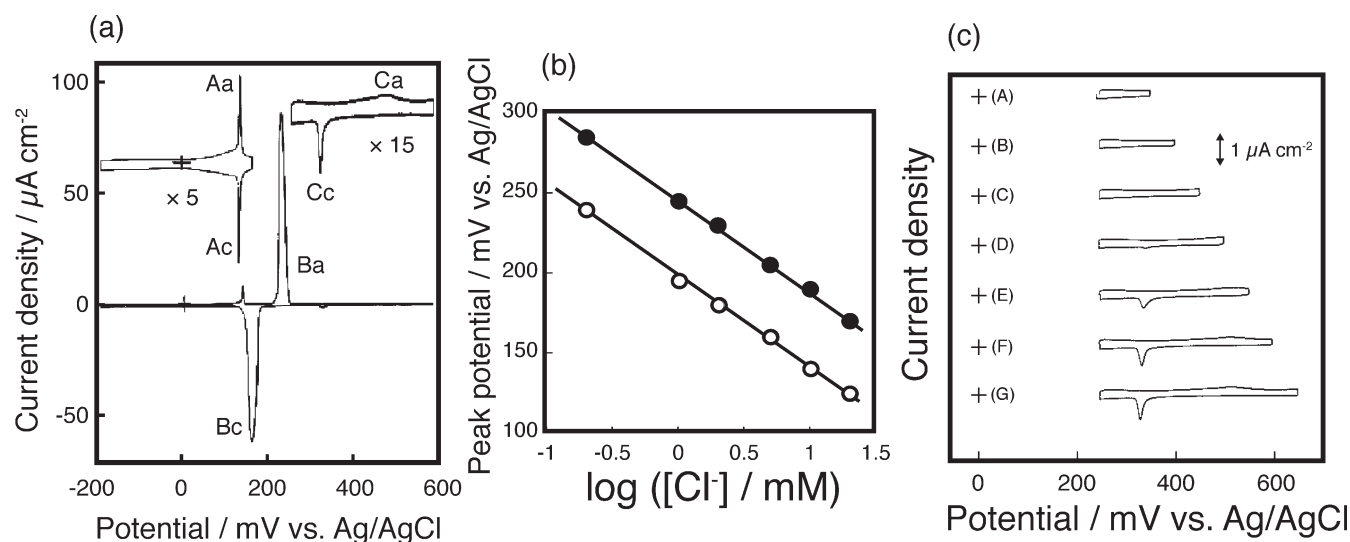
Figure 1. (a) CVs of the Ag(2 ML)/Au(111) electrode measured in a 50 mM H_2SO_4 aqueous solution containing 2 mM NaCl with a scan rate of 5 mV s^{-1}. Insets show expanded CVs obtained by scanning between −200 and +200 mV and between +250 and +580 mV. (b) Relationship between the peak potentials of anodic (closed circle) and cathodic (open circle) main peaks and the concentration of Cl$^-$ in the electrolyte solution. (c) CVs of the Ag(2 ML)/Au(111) electrode measured in a 50 mM H_2SO_4 aqueous solution containing 2 mM NaCl with a scan rate of 5 mV s^{-1} after the chlorination, obtained by scanning between +250 and (A) +350 mV, (B) +400 mV, (C) +450 mV, (D) +500 mV, (E) +550 mV, (F) +600 mV, and (G) +650 mV.

STM Measurements. STM observations were carried out on an atomically flat (111) facet of a gold single crystal bead, which was prepared by the Clavilier method.[41] STM measurements were carried out by using a NanoScope E (Digital Instrument) controller in the ECSTM mode with a homemade electrochemical STM cell, which can accommodate a single crystal bead electrode.[9,10,12,13,42] A Pt wire (diameter: 0.3 mm) and a Ag/AgCl electrode were used as a counter and a quasi-reference electrode, respectively. STM tips were simply cut Pt wire (diameter: 0.3 mm) insulated with nail polish. STM images were obtained in a constant current mode unless otherwise stated.

Prior to Ag UPD, the Au bead with (111) facets was annealed using a hydrogen flame, cooled in a quartz vessel for a few minutes, and then quenched in ultrapure water.[38] It was then transferred to a conventional electrochemical cell with a drop of ultrapure water on the surface to avoid any surface contamination. The Au bead electrode was contacted to a deaerated 50 mM H_2SO_4 aqueous solution containing 1 mM Ag_2SO_4 while keeping the potential at +700 mV (vs Ag/Ag$^+$), where no Ag is electrodeposited, and then 2 ML of Ag was deposited by scanning the potential from +700 to +10 mV with a scan rate of 5 mV s^{-1}.[15,16] After the deposition, the Ag(2 ML)/Au bead electrode was rinsed by ultrapure water, dried by blowing ultrapure N_2 gas, and then transferred to an ECSTM cell filled with 50 mM H_2SO_4 containing 2 mM NaCl. The Ag/AgCl reaction was carried out by scanning the potential between −200 mV (vs Ag/AgCl) and +600 mV.

SXS Measurements. A specially designed spectroelectrochemical cell made of Kel-F with a 6.0 μm thick Mylar film (Chemplex, D) window was used for in situ SXS measurements.[37,38] The spectroelectrochemical cell was set on a six-circle diffractometer (HUBER, 5020) installed in a bending-magnet beamline BL4C at Photon Factory or on a κ-type diffractometer (Newport) installed in a bending-magnet beamline BL14B1 at SPring-8.

A Ag(2 ML)/Au(111) disk, which was prepared in the conventional electrochemical cell as described in the Electrochemical Measurement section,[15,16] was used as a working electrode. After rinsing the Ag(2 ML)/Au(111) disk with ultrapure water, the disk

was set to the spectroelectrochemical cell.[37] A Pt wire (diameter: 0.3 mm) and a Ag/AgCl (sat. NaCl) electrode were used as a counter and a reference electrode, respectively. A 50 mM H_2SO_4 aqueous solution containing 2 mM NaCl was injected into the cell after being deaerated by passing the ultrapure N_2 or ultrapure Ar gas for more than 30 min while keeping the potential at −200 mV (vs Ag/AgCl), which was more negative than the potential where the anodic peaks were observed, and the Ag/AgCl reaction was then carried out.

Except for the dynamic study, the electrode potential was scanned in the thick layer configuration, in which the thickness of the electrolyte layer between the electrode surface and the Mylar window was more than 5 mm. After holding the electrode at a certain potential for more than 10 min in the thick layer configuration, the SXS measurements for the static structures were carried out in the thin layer configuration with the electrolyte thickness of ca. 30 μm so that X-ray scattering by the electrolyte layer becomes minimum.[38] It should be noted that for the measurements at +350 and +500 mV the potential was kept for more than 5 h at these potentials in the thick layer configuration before the SXS measurements were carried out because the structural changes at these potentials were much slower than those at other potentials as described later.

Dynamic SXS measurements for the potential-dependent interfacial structures were carried out in the slightly thicker layer configuration with the electrolyte thickness of ca. 100 μm.

The X-ray was monochromated by a Si(111) double crystal system and focused by a Rh-coated bending mirror. The beam size of the incident X-ray was 0.2 mm (vertical) × 0.2−0.5 mm (horizontal), which was adjusted by a slit placed in front of the cell. A wavelength of 1.100 Å was selected to avoid any fluorescence from the Au substrate. All the measurements were carried out under the configuration to ensure the incoming and outgoing angles with respect to the sample surface being equal. A reciprocal coordinate system (H, K, L) with two components (H and K) parallel to the surface and the other
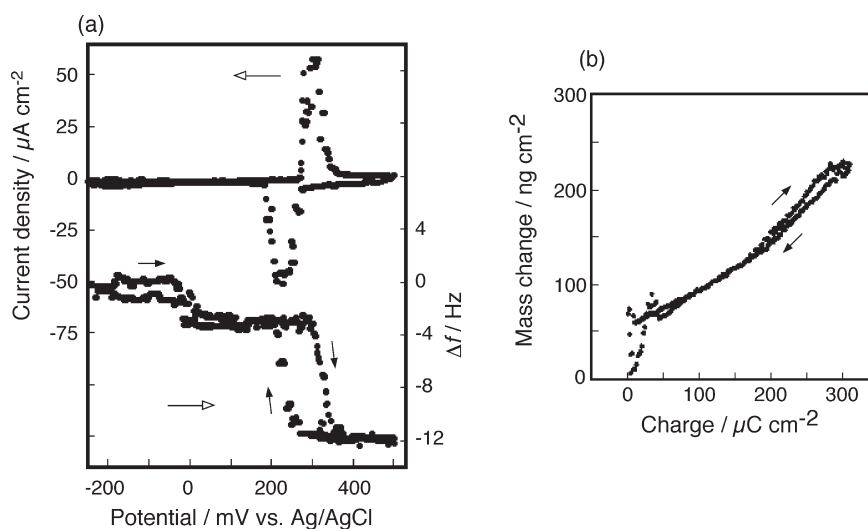
Figure 2. (a) Potential dependence of current and resonant frequency when the potential was swept between −220 and +500 mV with a scan rate of 20 mV s^{-1} in a 50 mM H$_2$SO$_4$ aqueous solution containing 2 mM NaCl. (b) Mass change calculated from resonant frequency change as a function of charge passed at the Ag(2 ML)/Au film electrode.

one (*L*) along the direction normal to the surface was used in this study.

In the present study, the (00) rod,[38] one of the crystal truncation rods (CTRs), and the surface X-ray diffraction (SXRD) curve were obtained to determine the interfacial structures normal and parallel, respectively, to the electrode surface. Structures normal to the surface were quantitatively determined from the least-squares fitting to the (00) rod data with a kinematic calculation.[11,38,43−45] All the fittings were carried out using the three-layer model on top of the Au(111) substrate. The amount of atoms in each layer is described by ML as a unit where 1 ML corresponds to 1.39 × 10^{15} atoms cm^{-2}.[15,38]

III. RESULTS AND DISCUSSION

Electrochemical Characteristics. Figure 1(a) shows cyclic voltammograms (CVs) of the Ag(2 ML)/Au(111) electrode measured in a 50 mM H$_2$SO$_4$ aqueous solution containing 2 mM NaCl with a scan rate of 5 mV s^{-1}. CVs in narrower potential ranges between −200 and +200 mV and between +250 and +580 mV with magnified current scales are also shown as insets. Three anodic peaks, a small sharp peak at +130 mV (peak **Aa**), a very large peak at +230 mV (peak **Ba**), and a very small broad peak at around +480 mV (peak **Ca**) and three cathodic peaks, a small sharp peak at +130 mV (peak **Ac**), a very large peak at +180 mV (peak **Bc**), and a sharp small peak at +330 mV (peak **Cc**), were observed. These peaks were repeatedly observed in the subsequent scans.

Peaks **Aa** and **Ac** were symmetric and appeared at the same potential. Current spikes similar to **Aa** and **Ac** have been observed at Ag(111) single crystal electrodes in electrolyte solutions containing the Cl$^-$ ion,[29−31] and Gewirth et al. showed that the spikes corresponded to the transition of the physorbed Cl$^-$ ion between disordered and ordered phases by in situ AFM.[30,31] Thus, the current spikes **Aa** and **Ac** should be due to a disorder/order phase transition of the adsorbed Cl$^-$ ion.

The peak potentials of the peaks **Ba** and **Bc** were linearly related with the logarithm of the Cl$^-$ concentration with a slope of ca. −60 mV/decade (Figure 1(b)), and both the anodic charge of the peak **Ba** and the cathodic charge of the peak **Bc** were

ca. 240 μC cm^{-2}, which is slightly larger than a value corresponding to 1 ML (222 μC cm^{-2}) for 1 electron reaction. These results suggest that a pair of the largest current peaks **Ba** and **Bc** correspond to the Ag/AgCl redox reaction (eq 1).

Figure 1(c) shows a set of CVs when the anodic potential scan limit was changed from +400 to +650 mV, while the negative potential scan limit was kept constant at +300 mV. A sharp cathodic peak at +330 mV (**Cc**) was observed only when the positive potential scan limit was more positive than +550 mV. A very broad anodic peak (**Ca**) was observed around +480 mV. These results suggest that the peak **Cc** corresponds to the reverse, i.e., reduction, reaction of the anodic reaction related to the peak **Ca**.

EQCM Measurements. Figure 2(a) shows the simultaneously recorded current and frequency change at the Ag(2 ML)/Au film EQCM electrode obtained in a 50 mM H$_2$SO$_4$ aqueous solution containing 2 mM NaCl while scanning the potential between −220 and +500 mV with a scan rate of 20 mV s^{-1}. A pair of anodic and cathodic peaks was observed at +300 and +220 mV, respectively, within this potential region. Although the peak positions were slightly different from those observed at the Ag(2 ML)/Au(111) electrode reported above, the former and the latter peaks should correspond to **Ba** and **Bc**, respectively. The charges corresponding to these peaks were ca. 300 μC cm^{-2}, which were slightly larger than those measured at the Ag(2 ML)/Au(111) electrode. The peaks corresponding to **Aa** and **Ac** were not observed. These results show that the evaporated Au film used as an electrode in the EQCM measurement was rougher and less ordered than the single crystal Au(111) electrode.

Clear frequency changes were observed around 0 mV and around +300 mV. Figure 2(b) shows the relation between the electric charge and mass change during the potential cycling shown in Figure 2(a). The frequency change around 0 mV was smaller and should correspond to adsorption/desorption of Cl$^-$.[29−31] Mass change in this potential region shows that ca. 1/3 ML of Cl$^-$ was adsorbed/desorbed. Since this mass change was not accompanied with current, the adsorption should be physisorption. The frequency change between +200 and +400 mV was much larger and should be due to the Ag/AgCl reaction depicted by eq 1 as the frequency change took place
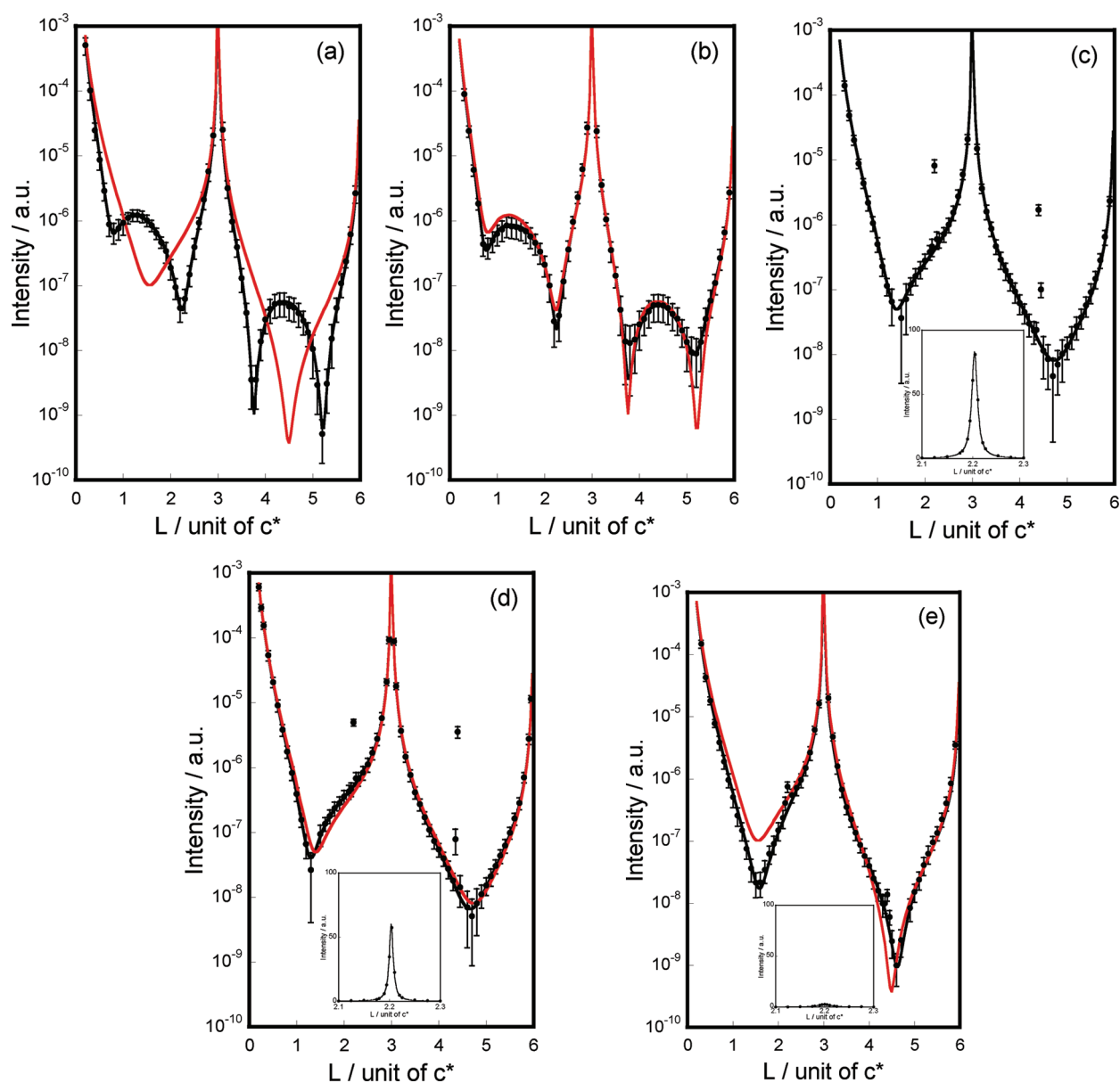
Figure 3. The (00) rod profiles of the Ag(2 ML)/Au(111) electrode measured in a 50 mM H_2SO_4 aqueous solution containing 2 mM NaCl at (a) -100 mV, (b) $+210$ mV, (c) $+350$ mV, (d) $+500$ mV, and (e) $+200$ mV after the reduction of AgCl. Black solid lines represent the fitted curves based on the simulation. Red solid lines represent the calculated curves. Details of the calculated models of red lines are described in the text. Insets: detailed diffraction profiles around $L = 2.2$.

when current due to the Ag/AgCl reaction flowed. Actually, a linear relation between the electric charge and mass change was obtained in this potential range (Figure 2(b)), and the mpe (mass per electron)[39,40] determined from the slope is ca. 58 g mol-electron^{-1}, suggesting that one Cl^- (35.5 g mol^{-1}) and $1-2$ water molecules (18 g mol^{-1}) were involved in the AgCl formation reaction.

Static Structures at Various Potentials. Figure 3 shows (00) rod data (closed circle) of the Ag(2 ML)/Au(111) electrode measured in a 50 mM H_2SO_4 aqueous solution containing 2 mM NaCl at various potentials and the best fit to the theoretical equation using the three-layer model (black solid line). Structural parameters obtained by the best fit are listed in Table 1.

(i). At -100 mV. Figure 3(a) shows the (00) rod of the Ag (2 ML)/Au(111) electrode obtained at -100 mV after the

electrode made contact with the electrolyte solution while keeping the potential at -200 mV. Two dips were observed between Bragg peaks ($L = 0, 3,$ and 6). The best fit data showed that the first, second, and third layers on the Au(111)-(1 × 1) substrate were 1.00 ML of Au, 1.00 ML of Ag, and 0.99 ML of Ag, respectively. All the parameters were exactly the same as those obtained for Ag(2 ML)/Au(111),[15] confirming that the pseudomorphic Ag UPD bilayer remained on the Au(111) surface even after the electrode was transferred from the Ag UPD preparation cell to the SXS cell without potential control[16] and the potential was scanned from -200 to -100 mV in the electrolyte solution. For a comparison, the simulated result for the Ag monolayer on the Au(111)-(1 × 1) surface is shown by a red curve in Figure 3(a). It is clear that not a Ag monolayer but a Ag bilayer was present on the Au(111) surface. The structure at -100 mV is schematically shown in Figure 4(a).

Table 1. Structure Parameters Obtained from the Analyses of the Reflectivity Profiles of the Ag(2 ML)/Au(111) Electrode Measured in a 50 mM H$_2$SO$_4$ Aqueous Solution Containing 2 mM NaCl at (a) −100 mV, (b) +210 mV, (c) +350 mV, (d) +500 mV, and (e) +200 mV after Reduction of AgCl

[a]	−100 mV	+210 mV	+350 mV	+500 mV	+200 mV
distance, z_{Au-Au}/Å	2.355 ± 0.003	-	2.355 ± 0.007	2.355 ± 0.005	2.355 ± 0.003
distance, z_{Au-Ag}/Å	2.356 ± 0.010	2.356 ± 0.023	2.278 ± 0.018	2.326 ± 0.020	2.356 ± 0.022
distance, z_{Ag-Ag}/Å	2.359 ± 0.009	2.359 ± 0.031	-	-	-
distance, z_{Ag-Cl}/Å	-	2.801 ± 0.108	0.925 ± 0.033	1.034 ± 0.025	2.779 ± 0.114
coverage, ρ_{Au}/ML	1.00 ± 0.01	-	1.00 ± 0.01	1.00 ± 0.01	1.00 ± 0.01
coverage, $\rho_{Ag(1)}$/ML	1.00 ± 0.01	1.00 ± 0.01	0.539 ± 0.028	0.562 ± 0.033	1.00 ± 0.029
coverage, $\rho_{Ag(2)}$/ML	0.99 ± 0.01	1.00 ± 0.01	-	-	-
coverage, ρ_{Cl}/ML	-	0.331 ± 0.022	0.541 ± 0.021	0.561 ± 0.039	0.334 ± 0.031
rms, σ_{Au}/Å	0.178 ± 0.005	-	0.086 ± 0.006	0.086 ± 0.010	0.091 ± 0.011
rms, $\sigma_{Ag(1)}$/Å	0.204 ± 0.033	0.245 ± 0.038	0.097 ± 0.013	0.102 ± 0.014	0.236 ± 0.016
rms, $\sigma_{Ag(2)}$/Å	0.393 ± 0.039	0.287 ± 0.042	-	-	-
rms, σ_{Cl}/Å	-	0.495 ± 0.098	0.588 ± 0.133	0.422 ± 0.102	0.102 ± 0.088

[a] Distances of z_{Au-Au}, z_{Au-Ag}, z_{Ag-Ag}, and z_{Ag-Cl} represent atomic layer distances between the Au substrate and the top Au layer, between the Au substrate and the Ag layer, between two Ag layers, and between the Ag and Cl layers, respectively.
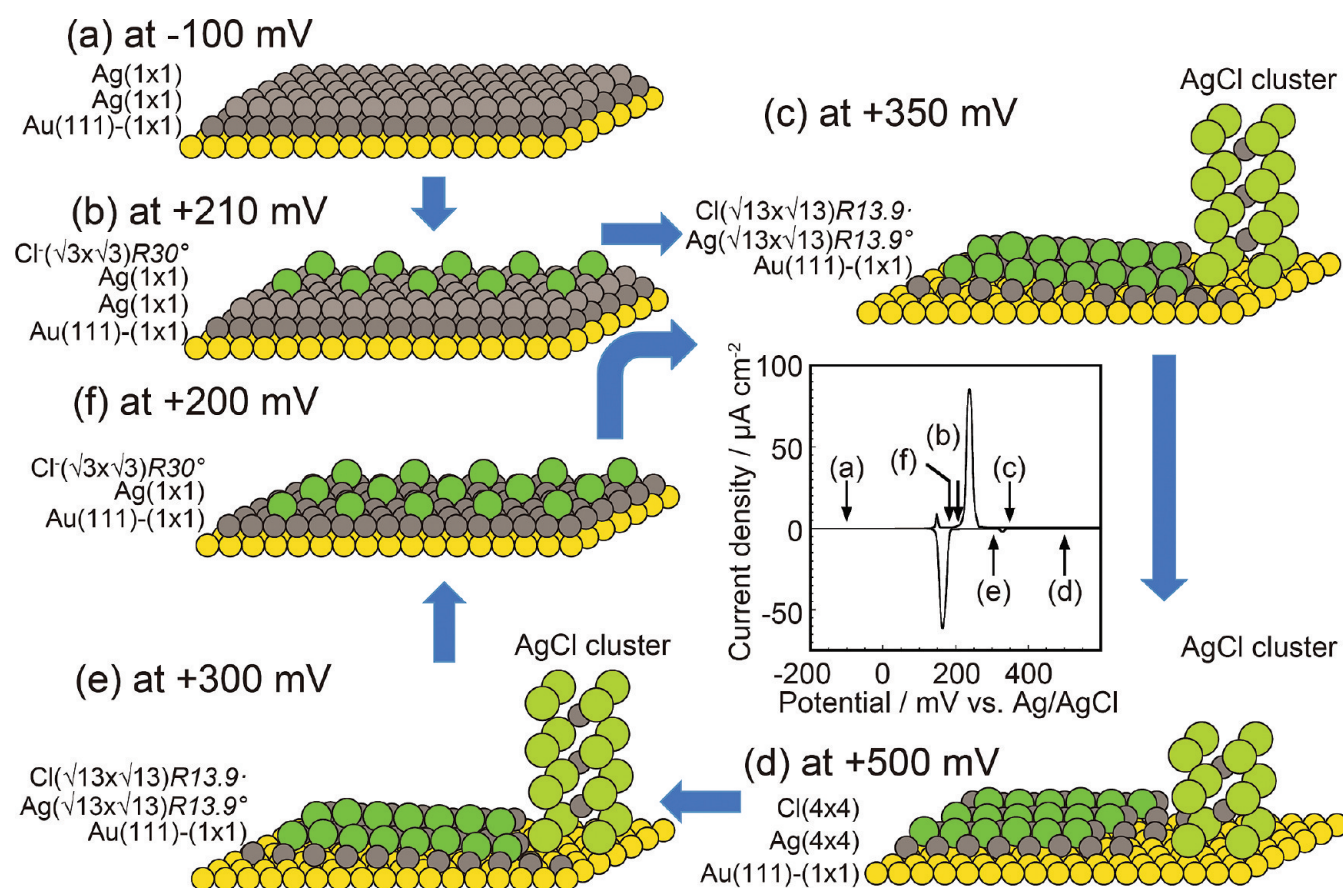
Figure 4. Schematic illustrations of the Ag(2 ML)/Au(111) electrode surfaces at various potentials with the CV of this electrode measured in a 50 mM H$_2$SO$_4$ aqueous solution containing 2 mM NaCl (Figure 1(a)).

(ii). At +210 mV. According to the best fit data to the (00) rod at +210 mV shown in Figure 3(b), which is between the potentials of two anodic peaks **Aa** and **Ba** (Figure 1(a)), the first, second, and third layers on the Au(111)-(1 × 1) substrate were 1.00 ML of Ag, 1.00 ML of Ag, and 0.33 ML of Cl, respectively, supporting the EQCM result that 1/3 ML of

Cl$^-$ ion was adsorbed on the Ag(2 ML)/Au(111) electrode surface. For a comparison, the simulated result for a Ag bilayer on a Au(111)-(1 × 1) surface without the Cl layer is also shown in Figure 3(b) by a red curve, which does not fit well to the experimental results. Thus, it is confirmed that 0.33 ML of Cl was indeed adsorbed on the Ag bilayer on the Au(111)-(1 × 1)

(a)

(b)

100 nm

5 nm
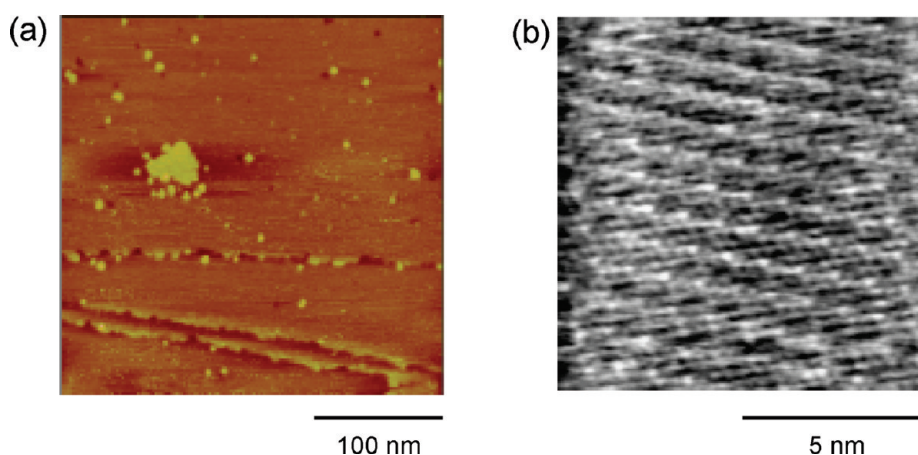
Figure 5. (a) Wide (300×300 nm^2) and (b) narrow (10×10 nm^2) STM images of the Ag(2 ML)/Au(111) electrode measured in a 50 mM H$_2$SO$_4$ aqueous solution containing 2 mM NaCl at +350 mV. E_{tip} = +400 mV and I_{tip} = 16.7 nA.

surface. The distance between the layers of the Cl$^-$ ion and Ag atoms was determined to be 2.8 Å (Table 1), revealing that Cl$^-$ ions were adsorbed at three hold-hollow sites of the underlying Ag(111) phase. The present result confirms the previous results of STM and SXS that adsorbed Cl$^-$ ions form the ($\sqrt{3} \times \sqrt{3}$) structure on a Ag(111) surface[29−32] as schematically shown in Figure 4(b).

(iii). At +350 mV. Figure 3(c) shows the (00) rod of the Ag(2 ML)/Au(111) electrode obtained at +350 mV, which is more positive than the peak **Ba**. A dip was observed between the Bragg peaks (L = 0, 3, and 6). In addition, intense peaks were observed at L = 2.2 and 4.4. Least squares fitting was carried out without taking into account these intense peaks, and the best fit data showed that the first, second, and third layers on the Au(111)-(1 × 1) substrate are 1.00 ML of Au, 0.54 ML of Ag, and 0.54 ML of Cl species, respectively, showing that the AgCl monolayer was present on the Au(111) surface at this potential. The position of the two intense peaks at L = 2.2 and 4.4 matched well with those of (200) and (400) reflections of AgCl bulk, indicating that AgCl monocrystalline clusters were also formed on the electrode surface at this potential. A detailed diffraction profile around L = 2.2 is shown in the inset of Figure 3(c). The size of the AgCl clusters formed at this potential was calculated to be ca. 260 Å by using the Scherrer equation.[46−49]

Figure 5 shows STM images in (a) wide (300×300 nm^2) and (b) narrow (10×10 nm^2) scan regions of the Ag(2 ML)/Au(111) electrode surface obtained at +350 mV in a 50 mM H$_2$SO$_4$ aqueous solution containing 2 mM NaCl. The wide scan image (Figure 5 (a)) shows the presence of nanoclusters on atomically flat terraces, confirming the CTR result, although the size of the nanoclusters in the STM image was less than that estimated by CTR. This discrepancy may be caused by the difference in the time required for the measurements. While it required more than 10 h to obtain one CTR, STM images were obtained only a few minutes after the potential was held at +350 mV. Nanoclusters may have grown during CTR measurements. The narrow scan image (Figure 5(b)) shows bright and dark spots with long-range order. The distance between the bright spots was ca. 10 Å, which is $\sqrt{13}$ times of the nearest neighbor (NN) atomic distance of the underlying Au atoms, 2.88 Å. The direction of the bright spot was different from that of the NN direction of the underlying Au atoms by ca. 14°, suggesting that the overlayer structure at this potential was ($\sqrt{13} \times \sqrt{13}$)$R$13.9° structure.

Figure 6(a) shows the SXRD profile measured along the K direction (H = 0 and L = 0.2) at +350 mV. A peak was observed at K = 0.734, showing that the Ag−Ag and Cl−Cl distances in the Ag and Cl layers, respectively, in the AgCl monolayer on Au(111) are 1/0.734 (= 1.36) times the NN atomic distance of underlying Au atoms, 2.88 Å, i.e., 3.92 Å. From this value, the coverage of the AgCl monolayer was calculated to be 0.54 ML, which confirmed the result of the (00) rod measurement mentioned above.

The directions of the Ag and Cl rows were determined by ϕ scan measurement, where ϕ is a rotating angle of the Au(111) disk electrode with respect to the axis normal to the surface. Figure 6(b) shows the SXRD profile as a function of ϕ (ϕ = 0° at H = 0 and K = 0.734), while $|H + K|$ was fixed as 0.734. Two broad peaks were obtained at ϕ = ±5.2°, indicating that the direction of rows of the AgCl monolayer was different from that of the underlying Au atoms by 5.2°. Two peaks were observed at both plus and minus ϕ sides in Figure 6(b), indicating that there were two kinds of 3-fold symmetric structures rotated clockwise and counterclockwise, respectively. The same result of the two broad peaks was also observed around (0.734 0), showing that both Ag and Cl atoms in the AgCl monolayer were in the 3-fold rotational symmetry.

A schematic model of the AgCl monolayer formed on the Au(111) surface based on the above results is shown in Figure 7(a). On the Au(111)-(1 × 1) surface, 0.54 ML of the Ag layer (Ag−Ag distance = 3.92 Å) with the atom row direction being 5.2° with respect to the underlying Au atoms was present. The outermost layer was 0.54 ML of Cl layer (Cl−Cl distance = 3.92 Å) with the atom row direction of 5.2° with respect to the underlying Au atoms. Cl atoms at the highest site in the outermost Cl layer represented by dark green circles formed the unit lattice of Au(111)-($\sqrt{13} \times \sqrt{13}$)$R$13.9° structure. The bright spots in the STM image (Figure 5(b)) should correspond to the Cl atoms at the highest site in the outermost Cl layer corresponding to the third nearest neighbor atoms. This structure can be considered as the ($\sqrt{7} \times \sqrt{7}$)R19.1° structure of the two-dimensional arrangement of Cl atoms. The atom−atom distances of Cl and Ag 3.92 Å were 1.36 times that of the underlying Au, i.e., 2.88 Å, as mentioned before, and 1.36 is equal to $\sqrt{13}$/$\sqrt{7}$. The size of the unit lattice, 10.37 Å, is equal to 3.92 Å × $\sqrt{7}$, which is in turn equal to 2.88 Å × $\sqrt{13}$, the distance between a Au atom and the fourth nearest neighbor atom in the underlying Au layer. The direction of the unit lattice with respect to
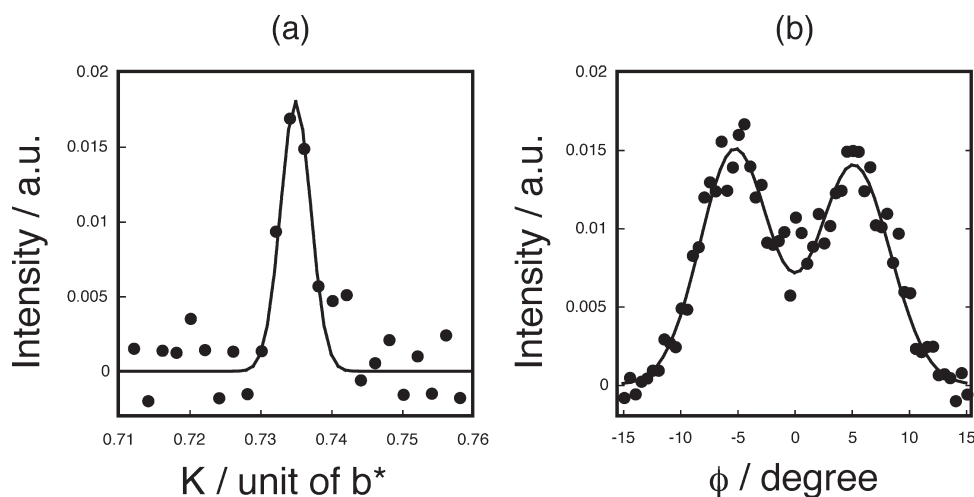
Figure 6. SXRD profiles of the Ag(2 ML)/Au(111) electrode measured in a 50 mM H_2SO_4 aqueous solution containing 2 mM NaCl at +350 mV along (a) the direction of K (at $H = 0$ and $L = 0.2$) and (b) the ϕ direction ($\phi = 0°$ at $(H\,K\,L) = (0\,0.735\,0.2)$). Solid lines represent the curves fitted by the Gaussian function.
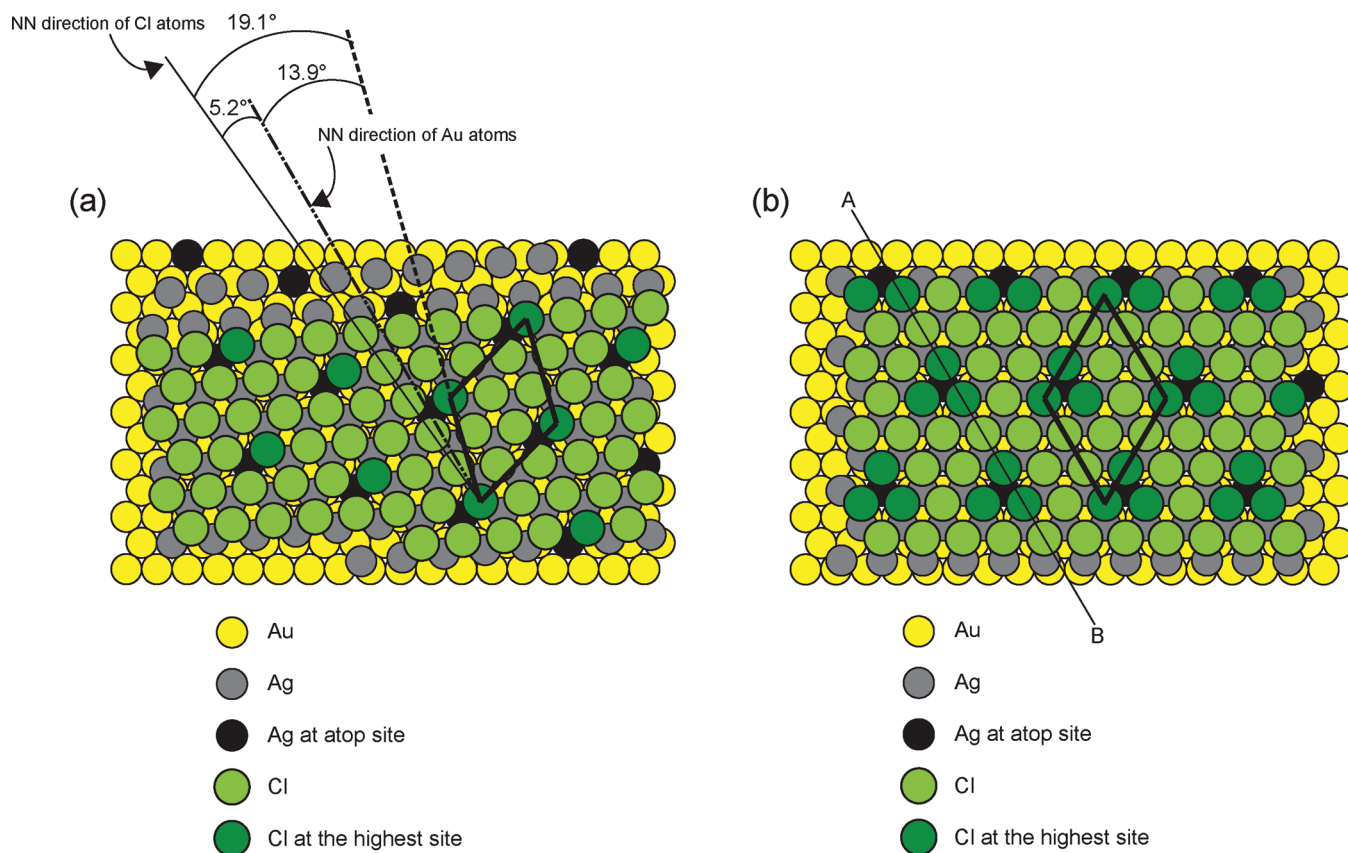

Figure 7. Top views of the models of (a) $(\sqrt{13} \times \sqrt{13})R13.9°$ and (b) (4×4) structures of the AgCl monolayer formed on the Au(111)-(1×1) surface.

underlying Au atoms was 13.9°, and that with respect to the atom row of Cl was 19.1°; therefore, the direction of the atom row of Cl with respect to underlying Au atoms should be 5.2° as experimentally observed. Thus, it is confirmed that the two-dimensional atomic arrangements of Ag and Cl in the AgCl monolayer formed at this potential were $(\sqrt{13} \times \sqrt{13})R13.9°$ structure. The NN distances of Cl and Ag in the Cl and Ag layers,

respectively, in this structure, 3.92 Å, are very close to those observed for the AgCl(111) surface, 3.93 Å,[50] indicating that the AgCl structure obtained at this potential was one of the most stable states of the AgCl crystal.

The interfacial structure at +350 mV including both the $(\sqrt{13} \times \sqrt{13})R13.9°$ structure and the AgCl monocrystalline cluster is schematically shown in Figure 4(c).
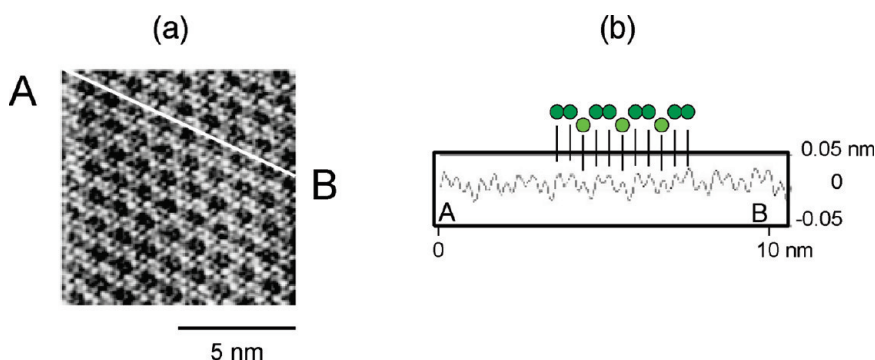
Figure 8. (a) STM image (10×10 nm^2) of the Ag(2 ML)/Au(111) electrode measured in a 50 mM H$_2$SO$_4$ aqueous solution containing 2 mM NaCl at +500 mV. E_{tip} = +550 mV and I_{tip} = 17.2 nA. (b) Cross section across the line A–B in Figure 8(a).

(iv). At +500 mV. Figure 3(d) shows the (00) rod of the Ag (2 ML)/Au(111) electrode obtained at +500 mV, which is slightly more positive than the peak **Ca**. A dip between Bragg peaks and the intense peaks at L = 2.2 and 4.4 was observed. The best fit data obtained without considering the intense peaks showed that the first, second, and third layers on the Au(111)-(1 × 1) substrate were 1.00 ML of Au, 0.56 ML of Ag, and 0.56 ML of Cl species, respectively. The coverage of the AgCl monolayer was 0.56 ML, which is slightly higher than 0.54 ML at +350 mV. Although the difference in the coverage between these two potentials was small, the difference between the best fitted curve for 0.56 ML (black) and the simulated curve for 0.54 ML on the Au(111) surface (red) is clearly seen in Figure 3(d). The presence of the two intense peaks at L = 2.2 and 4.4 corresponding to AgCl monocrystalline clusters showed that the AgCl monocrystalline clusters remained on the surface at this potential, although the detailed diffraction profile around L = 2.2 (the inset of Figure 3(d)) showed the size (ca. 220 Å), and the amount of AgCl clusters became smaller than those observed at +350 mV (ca. 260 Å). The presence of AgCl clusters was also confirmed by STM images of the wide scan region (not shown).

Figure 8(a) shows the STM image of 10 × 10 nm^2 regions at +500 mV. Bright and dark spots with long-range order were also observed as was the case for Figure 5(b), but the direction of the atomic arrangement was the same as that of the NN direction of the underlying Au atoms. The distance between the bright spots is 4 times the NN atomic distance of the underlying Au atoms, 2.88 Å. Figure 8(b) shows the cross-sectional image at the A–B line in Figure 8(a). Two higher atoms (open circles) and one lower atom (shadow circles) were alternately arranged in the outermost layer. These results suggest that the overlayer structure at this potential is (4 × 4) structure. Figure 9(a) shows the SXRD profile obtained by scanning in the K direction (H = 0 and L = 0.2) at +500 mV. A sharp peak was observed at K = 0.75, indicating that the Ag–Ag and Cl–Cl atomic–atomic distances in the AgCl monolayer on Au-(111) are 1/0.75 (= 1.33) times the NN distance of underlying Au, 2.88 Å, i.e., 3.83 Å, which is in good agreement with the value obtained by STM. From this value, the coverage of the AgCl monolayer was calculated to be 0.56 ML, which confirmed the value obtained from the (00) rod measurement.

Figure 9(b) shows the SXRD profile as a function of ϕ (ϕ = 0 at H = 0 and K = 0.75) while $|H + K|$ was fixed as 0.75. A sharp peak was observed at ϕ = 0°, indicating that the direction of the atomic row of the AgCl monolayer at this potential was exactly the same as that of the underlying Au atoms. Same sharp SXRD peaks were observed not only at (0 0.75) but also at (0 0.25), (0 0.50),

(0 1.00), (0.25 0), (0.25 0.25), (0.25 0.50), (0.25 0.75), (0.25 1.00), (0.50 0), (0.50 0.25), (0.50 0.50), (0.50 0.75), (0.50 1.00), (0.75 0), (0.75 0.25), (0.75 0.50), (0.75 0.75), (0.75 1.00), (1.00 0), (1.00 0.25), (1.00 0.50), (1.00 0.75), and (1.00 1.00), indicating that the structure of the AgCl monolayer at this potential should be (4 × 4), confirming the results of STM.

A schematic model of the AgCl monolayer formed on the Au(111) surface at +500 mV based on the above results, i.e., (4 × 4) structure, is shown in Figure 7(b). On the Au(111)-(1 × 1) surface, 0.56 ML of the Ag layer (Ag–Ag distance = 3.83 Å) with the atom row direction being equal to the underlying Au atoms was present. The outermost layer was 0.56 ML of the Cl layer (Cl–Cl distance = 3.83 Å) with the atom row direction equal to the underlying Au atoms. Cl atoms at the highest site in the outermost Cl layer represented by dark green circles formed the unit lattice of (4 × 4) structure. The bright spots in the STM image (Figure 8(a)) should correspond to the Cl atoms at the highest site in the outermost Cl layer, i.e., the third nearest neighbor atoms. This structure matches well with that of the cross sectional image (Figure 8(b)).

Diffraction peak intensity due to the AgCl cluster decreased, while the coverage of the AgCl monolayer increased as compared with those at +350 mV, suggesting that a small number of Ag and Cl atoms in the clusters join the monolayer to supply Ag and Cl atoms required to change the structure of the AgCl monolayer from ($\sqrt{13} \times \sqrt{13}$)$R13.9°$ structure to (4 × 4) structure, although the detailed mechanism of this potential induced phase transition is not clear.

The interfacial structure at +500 mV including both the (4 × 4) structure and the AgCl monocrystalline cluster is schematically shown in Figure 4(d).

(v). At +300 mV after the Formation of (4 × 4) Structure at +500 mV. The (00) rod profile and the SXRD patterns were obtained at +300 mV, which is more negative than +330 mV where the cathodic current peak **Cc** was observed (Figures 1(a) and 1(c)), after the formation of the (4 × 4) structure of the AgCl monolayer at 500 mV, and potential was scanned back negatively. They were exactly the same as those observed at +350 mV before the formation of (4 × 4) structure (Figure 3(c) for CTR and Figures 6(a) and 6(b) for SXRD patterns), showing that the AgCl monolayer of ($\sqrt{13} \times \sqrt{13}$)$R13.9°$ structure with the AgCl monocrystalline cluster was formed again at this potential as schematically shown in Figure 4(e).

(vi). At +200 mV after One Cycle. After AgCl was formed on the Au(111) surface and was then electrochemically reduced at the potential more negative than that of the peak **Bc** (+180 mV), the (00) rod was monitored at +200 mV (Figure 3(e)). At this

(a)

(b)
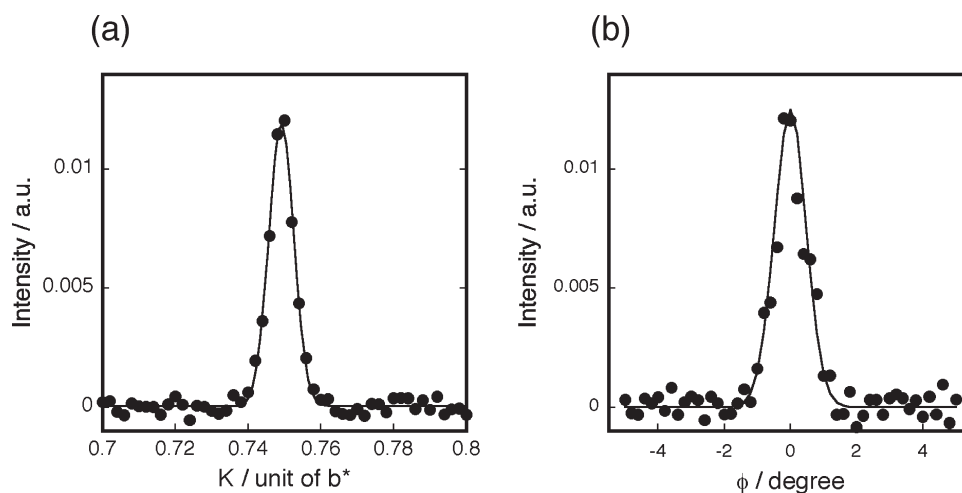
Figure 9. SXRD profiles of the Ag(2 ML)/Au(111) electrode measured in a 50 mM H$_2$SO$_4$ aqueous solution containing 2 mM NaCl at +500 mV along (a) the direction of K (at H = 0 and L = 0.2) and (b) the ϕ direction (ϕ = 0° at ($H K L$) = (0 0.75 0.2)). Solid lines represent the curves fitted by the Gaussian function.
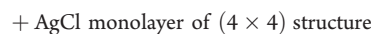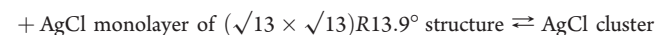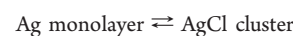
(a)

(b)

(c)
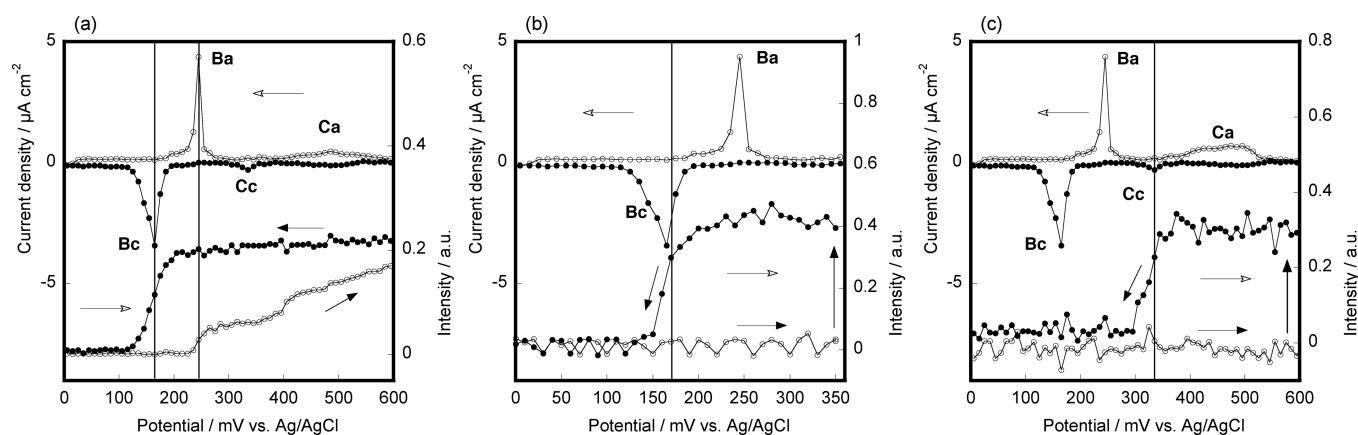
Figure 10. Potential dependence of current and X-ray scattering intensity at (a) (0 0 2.2), (b) (0 0.735 0.2), and (c) (0 0.75 0.2) obtained in a 50 mM H$_2$SO$_4$ aqueous solution containing 2 mM NaCl while sweeping potential with 1 mV s^{-1}. Open and closed circles represent the data obtained in the positive and negative going scans, respectively. Potentials were kept at (a) +600 mV for 1 min, (b) +350 mV for 5 h, and (c) +600 mV for 5 h with the electrolyte thickness of ca. 300 μm before the negative going scans were started.

potential, the best fit data showed that the first, second, and third layers on the Au(111)-(1 × 1) substrate were 1.00 ML of Au, 1.00 ML of Ag, and 0.33 ML of Cl species, respectively, indicating that the Ag bilayer was not recovered but that a Ag monolayer was formed on the Au(111) surface once the AgCl phase was formed. For a comparison, the simulated result for the Ag monolayer on the Au(111)-(1 × 1) surface without a Cl layer is also shown in Figure 3(e) by a red curve, which does not fit well to the experimental results. Thus, it is confirmed that 0.33 ML of Cl was indeed adsorbed on the Ag monolayer on the Au(111)-(1 × 1) surface. Ag atoms equivalent to 1 ML were missing. Although the presence of two peaks at L = 2.2 and 4.4 in Figure 3(e) after the reduction of AgCl shows some of them still remained as AgCl clusters on the Au(111) surface, the intensities of these peaks were much smaller than those observed before the AgCl reduction (Figure 3(c) and (d)), showing some of the Ag atoms were left in the solution after being reduced. The interfacial structure at this potential is schematically shown in Figure 4(f).

(vii). Structures in the Subsequent Potential Cycles. SXS measurements at +200, +350, and +500 mV when the potential

was varied positively and at +350 and +200 mV when the potential was varied negatively in the subsequent potential cycles showed that the conversion of

Ag monolayer $\rightleftarrows$ AgCl cluster

+ AgCl monolayer of ($\sqrt{13} \times \sqrt{13}$)$R$13.9° structure $\rightleftarrows$ AgCl cluster

+ AgCl monolayer of (4 × 4) structure

took place repeatedly.

Dynamics of Structural Changes. Dynamics measurements were carried out in the slightly thicker layer configuration with a potential scan rate of 1 mV s^{-1}. Figure 10 shows potential dependences of currents and X-ray scattering intensities at (a) (0 0 2.2) corresponding to the (200) AgCl reflection peak of the AgCl cluster, (b) (0 0.734 0.2) corresponding to the SXRD peak of the AgCl monolayer of ($\sqrt{13} \times \sqrt{13}$)$R$13.9° structure observed in Figure 6(a), and (c) (0 0.75 0.2) corresponding to the SXRD peak due to the AgCl monolayer of (4 × 4) structure observed in Figure 9(a). The potential scan was started from 0 V to the positive direction in all cases.

In the positive going potential scan, the intensity at $(0\ 0\ 2.2)$ (Figure 10(a)) was zero between 0 and $+230$ mV and was gradually increased from $+230$ mV where the anodic peak **Ba** was observed. The intensity increased more if the potential was kept at $+600$ mV for a few minutes. After the intensity reached constant at $+600$ mV, the negative going potential scan was started. The intensity was constant until the potential reached $+200$ mV and then decreased to nearly zero as the cathodic current flowed accompanied with the cathodic peak **Bc**. The intensity at $(0\ 0.734\ 0.2)$ (Figure 10(b)) was nearly zero in the whole potential range $(0-350\ mV)$ in the positive going potential scan even after the potential reached $+350$ mV, although the anodic peak **Ba** was observed at $+230$ mV, but it became significant if the potential was kept at $+350$ mV for more than 5 h with an electrolyte thickness of ca. 300 μm, showing that $(\sqrt{13} \times \sqrt{13})R13.9°$ structure was formed. Once the intensity became constant, i.e., the formation of the $(\sqrt{13} \times \sqrt{13})R13.9°$ structure was completed, the negative going potential scan was started. In the negative going potential scan, the intensity was constant until potential reached $+200$ mV and then decreased to zero associated with cathodic current flow corresponding to the peak **Bc**.

Thus, a pair of current peaks **Ba** and **Bc** should correspond to the conversion of Ag to AgCl, i.e., Ag/AgCl reaction. When the anodic current corresponding to the anodic peak **Ba** flowed, Ag was anodically converted to AgCl; however, it took a long time for the AgCl clusters to grow, and much longer time was required for the ordered AgCl monolayer with $(\sqrt{13} \times \sqrt{13})R13.9°$ structure to be formed. Reflection peaks due to AgCl clusters, $(0\ 0\ 2.2)$, and the AgCl monolayer of $(\sqrt{13} \times \sqrt{13})R13.9°$ structure, $(0\ 0.734\ 0.2)$, disappeared as soon as the cathodic peak corresponding to the peak **Bc** flowed simply because AgCl was converted to Ag.

The intensity at $(0\ 0.75\ 0.2)$ (Figure 10(c)) was nearly zero in the whole potential range $(0-600\ mV)$ in the positive going potential scan even after the potential reached $+600$ mV, although the anodic peaks at $+230$ mV, **Ba**, and at $+480$ mV, **Ca**, were observed, but it became significant, showing the formation of (4×4) structure if the potential was kept at $+600$ mV for more than 5 h with an electrolyte thickness of ca. 300 μm. When the intensity became constant, i.e., the formation of the (4×4) structure was completed, the negative going potential scan was started. In the negative going potential scan, the intensity was constant until $+350$ mV but decreased to zero as the cathodic current associated with the small cathodic peak **Cc** flowed. Considering the results of the above and of Figure 1(c), a pair of peaks **Ca** and **Cc** should correspond to the conversion of the AgCl structure between $(\sqrt{13} \times \sqrt{13})R13.9°$ and (4×4) structures. The anodic conversion of the $(\sqrt{13} \times \sqrt{13})R13.9°$ structure to the (4×4) structure is much slower than the cathodic conversion of the (4×4) structure to the $(\sqrt{13} \times \sqrt{13})$-$R13.9°$ structure in agreement with the broad **Ca** peak and sharp **Cc** peak (Figure 1). A slower anodic process than the cathodic one may be due to the fact that more AgCl must be incorporated into the ordered lattice in the anodic process, while the less dense structure is formed in the cathodic process.

IV. CONCLUSIONS

The Ag/AgCl reaction at the Ag UPD bilayer prepared on a Au(111) surface was investigated using electrochemical quartz crystal microbalance (EQCM), scanning tunneling microscopy (STM), surface X-ray scattering (SXS), and electrochemical techniques. The Ag bilayer on the Au(111) surface was anodically converted to AgCl in an electrolyte solution containing 2 mM Cl$^-$ when the potential more positive than $+230$ mV (vs Ag/AgCl, sat. NaCl), at which the anodic current peak due to the chlorination was observed, was applied. STM and SXS measurements showed the formation of AgCl clusters and the AgCl monolayer of $(\sqrt{13} \times \sqrt{13})R13.9°$ structure, although the former and the latter were formed slowly and very slowly, respectively. The AgCl monolayer of $(\sqrt{13} \times \sqrt{13})R13.9°$ structure was transformed to the AgCl monolayer of (4×4) structure when the potential more positive than $+480$ mV (vs Ag/AgCl, sat. NaCl), at which a very broad anodic current peak was observed, was applied for prolonged time. The AgCl monolayer of (4×4) structure was returned to the AgCl monolayer of $(\sqrt{13} \times \sqrt{13})R13.9°$ structure when the potential became more negative than $+330$ mV, at which a sharp cathodic current peak was observed. Both AgCl clusters and the AgCl monolayer of the $(\sqrt{13} \times \sqrt{13})R13.9°$ structure disappeared, and the Ag monolayer, not bilayer, was formed on the Au(111) surface when the potential became more negative than $+180$ mV, where a very large cathodic peak was observed.

In the subsequent potential cycles between 0 and $+600$ mV, the conversion of

$$\text{Ag monolayer} \rightleftarrows \text{AgCl cluster}$$

$$+ \text{AgCl monolayer of } (\sqrt{13} \times \sqrt{13})R13.9° \text{ structure} \rightleftarrows \text{AgCl cluster}$$

$$+ \text{AgCl monolayer of } (4 \times 4) \text{ structure}$$

took place repeatedly, although the formations of the AgCl cluster and the ordered structures were rather slow.

■ AUTHOR INFORMATION

Corresponding Author

*Tel.: $+81$-29-860-4301. Fax: $+81$-29-851-3362. E-mail: uosaki.kohei@nims.go.jp.

■ ACKNOWLEDGMENT

■ REFERENCES

(1) Abruña, H. D. *Electrochemical Interfaces: Modern Techniques for In Situ Interfacial Characterization*; VCH Publishers, Inc.: New York, 1991.

(2) Chen, C. J. *Introduction to Scanning Tunneling Microscopy*; Oxford University Press: New York, 1993.

(3) Somorjai, G. A. *Surface Chemistry and Catalysis*; John Wiley & Sons: New York, 1990.

(4) Adamason, A. W. *Physical Chemistry of Surface*, 4th ed.; John Wiley & Sons: New York, 1994.

(5) Argile, C.; Rhead, G. E. *Surf. Sci. Rep* **1989**, *10*, 277–356.

(6) Brune, H. *Surf. Sci. Rep* **1998**, *31*, 121–229.

(7) Capper, P.; Irvine, S.; Joyce, T. In *Springer Handbook of Electronic and Photonic Materials*; Kasap, S., Capper, P., Eds.; Springer-Verlag: Heidelberg, 2006.

(8) Uosaki, K.; Ye, S.; Kondo, T.; Naohara, H. In *Thin Films: Preparation, Characterization, Applications*; Soriaga, M. P., Stickney, J., Bottomley, L. A., Kim, Y.-G., Eds.; Kluwer Academic/Plenum Publishers: New York, 2002.

(9) Naohara, H.; Ye, S.; Uosaki, K. *J. Electroanal. Chem.* **2001**, *500*, 435–445.

(10) Naohara, H.; Ye, S.; Uosaki, K. *Electrochim. Acta* **2000**, *45*, 3305–3309.

(11) Takahasi, M.; Hayashi, Y.; Mizuki, J.; Tamura, K.; Kondo, T.; Naohara, H.; Uosaki, K. *Surf. Sci.* **2000**, *461*, 213–218.

(12) Naohara, H.; Ye, S.; Uosaki, K. *Appl. Phys. A: Mater. Sci. Process.* **1998**, *66*, S457–S461.

(13) Naohara, H.; Ye, S.; Uosaki, K. *J. Phys. Chem. B* **1998**, *102*, 4366–4373.

(14) Takahasi, M.; Tamura, K.; Mizuki, J.; Kondo, T.; Uosaki, K. *J. Phys. Condens. Matter* **2010**, *22* (474002), 9p.

(15) Kondo, T.; Morita, J.; Okamura, M.; Saito, T.; Uosaki, K. *J. Electroanal. Chem.* **2002**, *532*, 201–205.

(16) Kondo, T.; Takakusagi, S.; Uosaki, K. *Electrochem. Commun.* **2009**, *11*, 804–807.

(17) Schott, J. H.; White, H. S. *Langmuir* **1994**, *10*, 486–491.

(18) Schott, J. H.; White, H. S. *J. Phys. Chem.* **1994**, *98*, 291–296.

(19) Schott, J. H.; White, H. S. *J. Phys. Chem.* **1994**, *98*, 297–302.

(20) Kawasaki, M.; Ishii, H. *Langmuir* **1995**, *11*, 832–841.

(21) Rovida, G.; Pratesi, F. *Surf. Sci.* **1975**, *51*, 270–282.

(22) Goddard, P. J.; Lambert, R. M. *Surf. Sci.* **1977**, *67*, 180–194.

(23) Bowker, M.; Waugh, K. C. *Surf. Sci.* **1983**, *134*, 639–664.

(24) Lamble, G. M.; Brooks, R. S.; Ferrer, S.; King, D. A. *Phys. Rev. B* **1986**, *34*, 2975–2978.

(25) Zei, M. S. *J. Electroanal. Chem.* **1991**, *308*, 295–307.

(26) Hecht, D.; Strehblow, H. H. *J. Electroanal. Chem.* **1997**, *436*, 109–118.

(27) Andrshechkin, B. V.; Eltsov, K. N.; Shevlyuga, V. M.; Yurov, V. Y. *Surf. Sci.* **1998**, *407*, L633–L639.

(28) Andrsechkin, B. V.; Eltsov, K. N.; Shevlyuga, V. M. *Surf. Sci.* **1999**, *433–435*, 109–113.

(29) Aloisi, G.; Funtikov, A. M.; Will, T. *J. Electroanal. Chem.* **1994**, *370*, 297–300.

(30) Sneddon, D. D.; Gewirth, A. A. *Surf. Sci.* **1995**, *343*, 185–200.

(31) Sneddon, D. D.; Sabel, D. M.; Gewirth, A. A. *J. Electrochem. Soc.* **1995**, *142*, 3027–3033.

(32) Ocko, B. M.; Mugnussen, O. M.; Wang, J. X.; Adzic, R. R.; Wandlowski, Th. *Phys. B* **1996**, *221*, 238–244.

(33) Si, S. K.; Gewirth, A. A. *Phys. Chem. Chem. Phys.* **2001**, *3*, 3325–3329.

(34) Shimooka, T.; Inukai, J.; Itaya, K. *J. Electrochem. Soc.* **2002**, *149*, E19–E25.

(35) Bozzini, B.; Giovannelli, G.; Mele, C. *Surf. Coat. Technol.* **2007**, *202*, 4619–4627.

(36) Ye, S.; Ishibashi, C.; Uosaki, K. *Langmuir* **1999**, *15*, 807–812.

(37) Kondo, T.; Tamura, K.; Takahasi, M.; Mizuki, J.; Uosaki, K. *Electrochim. Acta* **2002**, *47*, 3075–3080.

(38) Kondo, T.; Morita, J.; Hanaoka, K.; Takakusagi, S.; Tamura, K.; Takahasi, M.; Mizuki, J.; Uosaki, K. *J. Phys. Chem. C* **2007**, *111*, 13197–13204.

(39) Ye, S.; Haba, T.; Sato, Y.; Shimazu, K.; Uosaki, K. *Phys. Chem. Chem. Phys.* **1999**, *1*, 3653–3659.

(40) Sauerbrey, G. Z. *Z. Phys.* **1959**, *155*, 206–222.

(41) Clavilier, J.; Faure, R.; Guinet, G.; Durand, R. *J. Electroanal. Chem.* **1980**, *107*, 205–209.

(42) Takakusagi, S.; Kitamura, K.; Uosaki, K. *J. Phys. Chem. C* **2008**, *112*, 3073–3077.

(43) Feidenhans'l, R. *Surf. Sci. Rep.* **1989**, *10*, 105–188.

(44) Gibbs, D.; Ocko, B. M.; Zehner, D. M.; Mochrie, S. G. *J. Phys. Rev. B* **1988**, *38*, 7303–7310.

(45) Wang, J.; Ocko, B. M.; Davenport, A. J.; Isaacs, H. S. *Phys. Rev. B* **1992**, *46*, 10321–10338.

(46) Scherrer, P. *Nachr. Ges. Wiss. Göttingen* **1918**, *2*, 96–100.

(47) Klug, H. P.; Alexander, L. E. *X-ray Diffraction Procedures for Polycrystalline and Amorphous Materials*, 2nd ed.; Wiley: New York, 1974.

(48) Borchert, H.; Shevchenko, E. V.; Robert, A.; Mekis, I.; Kornowski, A.; Grübel, G.; Weller, H. *Langmuir* **2005**, *21*, 1931–1936.

(49) Waje, S. B.; Hashim, M.; Yusoff, W. D. W.; Abbas, Z. *Appl. Surf. Sci.* **2010**, *256*, 3122–3127.

(50) Swanson, H. E.; Fuyat, R. K.; Ugrinic, G. M. *Natl. Bur. Stand. Circ. (U.S.)* **1955**, *539*, 75.